A NOVEL APPROACH OF OBTAINING OPTIMAL SOLUTION FOR E-SPIRIT

Ifat Al Baqee[1]

***Abstract*—** Magnetic Resonance Imaging (MRI) is an emerging technology in the field of medical imaging, which reduced the need to use invasive imaging technologies like computed tomography. As the image acquiring process behind the MRI technology is complex physics, the focus has been given to simplifying and enhancing the efficacy of the MRI technology. In this work, the focus has been given to an already recognized parallel MRI (pMRI) reconstruction method named Eigenvalue Iterative Self-Consistent Parallel Imaging Reconstruction or ESPIRiT. ESPIRiT uses coil-by-coil parallel reconstruction procedure along with Eigenvalue decomposition for sensitivity like estimation and then utilizes traditional sum-of-square (SOS) to reconstruct the final MR image. The SOS recombination technique proved to be augmenting noise as well as it based on the assumption that parallel coil sensitivities are uniform. In this work a convex optimization outline has been proposed which can replace the SOS recombination technique as well as can deliver an optimal solution for ESPIRiT. The SOS recombination of ESPIRiT has been replaced by a convex optimization formula and the modified convex ESPIRiT has been compared with the original ESPIRiT for demonstrating efficacy. The comparison results comprise qualitative, quantitative, and noise-based analysis to illustrate the efficiency of the proposed formula.

***Keywords*—**g-factor maps, Auto-calibration, sensitivity maps, ESPIRiT, iterative optimization, convex optimization, global solution sum-of-square (SOS), artifacts

I. INTRODUCTION

MAGNETIC Resonance Imaging (MRI) is a technique that employs a magnetic field and radio frequency signals to create detailed information of the living organs and tissues. The development of MRI transformed medical imaging technology which quickly became a noninvasive medical imaging procedure. Since its development, doctors and researchers have combined many modern techniques to use MRI scans to assist in imaging procedures and help in research [1]. Recent research focuses have been concentrated on the fact to improve clinical impacts and efficiencies such as faster scanning times, improved throughput with better quality of reconstruction.

The advent of parallel MRI (pMRI) acquisition improved the spatiotemporal resolution of MRI in both anatomical and functional scans. Parallel MRI employs a Radio-Frequency or RF coil array to concurrently obtain samples from multiple receivers, and data reduction is attained by reducing phase-encoding samples along the k-space trajectory [2]. The pMRI reconstruction is based on the subsampled k-space data (frequency data) and requires information on the spatial sensitivity functions of the receiver coil array. Based on how the coil sensitivity functions are preserved and incorporated into the pMRI reconstruction, the existing reconstruction algorithms may be subdivided into multiple categories.

One of the popular technology and well adopted by many imaging tech industries for pMRI reconstruction is based on the auto-calibration data from a pre reference scan and the sum-of-squares (SOS) action [2]. Using the subsampled k-space data, the auto-calibration process reconstructs a complete set of k-space data for each coil followed by an inverse discrete Fourier transform or DFT to acquire the corresponding sensitivity encoded image. Or it may directly yield the sensitivity encoded matrix of the coil in the spatial domain. Explicit values of the coil sensitivity functions are not needed in the auto-calibration-based methods. The SOS recombination technique is further implemented to the acquired sensitivity encoded image functions to complete the image reconstruction. The SOS operation only delivers the magnitudes of the complex-valued image. So, it provides a final pMRI image with magnitude data only but does not provide any phase information. Typical algorithms of this category are GRAPPA [3], IIR GRAPPA [4], and other similar methods, which perform interpolation of the auto-calibrating signal lines (ACS) in the k-space. Some recent algorithms perform the auto-calibration by regularized optimization, e.g. [5], [6], [7], and [8], or by eigenvalue decomposition, e.g. [9]. The obvious benefit of the aforesaid coil-by-coil reconstruction method is they are more resistant to errors in sensitivity coil data

I. A. Baqee is with the Department of Electrical and Electronic Engineering, Southeast University, Dhaka, Bangladesh (e-mail: *ifat.albaqee@seu.edu.bd*).

and embody less visible artifacts [10], [11], and [12] but tend to omit phase information in the final MR image and also noise accumulation is higher due to SOS operation.

The inspiration for this work has been drawn from the fact that the coil data SOS recombination technique results from more noise in the final MR image. In this work, a convex optimization-based method has been employed to substitute the SOS operation used in the aforementioned group of algorithms. It has been also examined through proper means whether replacing SOS operation with convex optimization yields a better outcome or not. Thorough comparisons and noise analysis has been done. For analytical judgments, Eigenvalue decomposition Iterative Self-Consistent Parallel Imaging Reconstruction from Arbitrary k-Space or conjugate gradient or ESPIRiT [9], which is a blend of auto-calibration and sensitivity approximation, has been nominated. It uses iterative optimization to produce the coil images and then employs SOS for recombining the coil images into the final desired image. In this work, the SOS technique is being replaced by a convex optimization-based approach [13] to obtain a truly optimal solution and a final MR image that is more insusceptible to noise. Appropriate comparisons have been done subsequently.

In this paper, $\mathbb{R}$, $\mathbb{R}_+$ and $\mathbb{C}$ indicates the sets of real, non-negative real, and complex numbers, correspondingly. The lower case letter in bold character symbolizes vectors and the capital case letter in bold character denotes matrices. $\succcurlyeq$ and $\preccurlyeq$ symbolize the elementwise operations of $\geq$ and $\leq$ on vectors, respectively. $\odot$ denotes the Hadamard or elementwise product of vectors and $|\cdot|$ means the elementwise magnitude of vector data.

II. Theory And Methodology

A. A General Framework of ESPIRiT

An eigenvalue approach to auto-calibrating parallel MRI: where SENSE meets GRAPPA or ESPIRiT was proposed in 2014 [9], which opts to bridge the gap between SENSE and GRAPPA by using the advantages of both the methods in a SPIRiT [5] type reconstruction. Authors derived a relation between the eigenvectors of the auto-calibration matrix used in GRAPPA and the sensitivity functions used in SENSE, assuming that both SENSE and GRAPPA are subspace-based methods that perform the pMRI reconstruction by recovering the solutions from a subspace. Instead of computing the coil maps through a traditional reference scan, eigenvalue vectors from auto-calibration operators in the k-space domain are used to derive the sensitivity maps through eigenvalue decomposition in image space. Then these estimated coil maps are used for pMRI reconstruction by SENSE-like algorithm, the process overcomes the limitations of auto-calibration-based methods.

A typical representation of an MRI equation can be written as

$$u_l = RF\, s_l\, I_m \dots\dots\dots\dots\dots\dots\dots\dots\dots\dots (1)$$

Where, u_l represents the acquired subsampled k-space pMRI dataset, l=1, 2, 3,…, L represents the pMRI coil array, R denotes the subsampling domain matrix, F represents the Fourier domain, s_l indicates the sensitivity maps and I_m is the original slice image. Equation (1) is used by SENSE using pre-estimated coil maps. For images for each coil, the sensitivity encoded images can be represented as

$$I_{ml} = s_l\, I_m \dots\dots\dots\dots\dots\dots\dots\dots\dots\dots (2)$$

As the inspiration of ESPIRiT is mainly from GRAPPA [3], let's present the interpolation scheme used by GRAPPA

$$I_{ml}(r) = (R_r B_r u)^T n_l^r \dots\dots\dots\dots\dots\dots\dots\dots\dots\dots (3)$$

Where, r indicates a particular position, B_r stands for a reconstruction block, $(\,)^T$ is the transpose of a matrix, u is the vectored representation of stacked u_l, n_l^r is the GRAPPA reconstruction weights, also known as the auto-calibration kernels for position r.

Reconstruction weights are usually derived by

$$u_l^{AC} = R_r^T\, B_A n_l^r \dots\dots\dots\dots\dots\dots\dots\dots\dots\dots (4)$$

where, u_l^{AC} is the fully acquired samples for auto-calibration, B_A is the selected matrix block in the k-space for auto-calibration. u_l^{AC} can be expressed as

$$u_l^{AC} = B_A a_i$$

Where, a_i selects the i-th coil data from the auto-calibration matrix. Now, equation estimation of the reconstruction weights is expressed as

$$B_A a_i = R_r^T B_A n_l^r$$

$$or\ B_A(R_r^T n_l^r - a_i) = 0 \dots\dots\dots\dots\dots\dots\dots\dots (5)$$

The authors have proved in [9] through singular value decomposition (SVD) on auto-calibration block matrix B_A that there exists a Hermitian and positive semi-definite matrix ξ with eigenvalues smaller or equal to one, which satisfies the following condition

$$\xi I_m{}^\star = I_m{}^\star \dots\dots\dots\dots\dots\dots\dots\dots\dots\dots (6)$$

$I_m{}^\star$ being a possible solution.

From SENSE based reconstruction framework, solution $I_m{}^\star$ in the k-space domain is depicted as

$$I_{mk}{}^\star = FSI_m{}^\star \dots\dots\dots\dots\dots\dots\dots\dots (7)$$

Where, $S = [s_1, s_2, \dots\dots, s_l]^T$ is the stacked coil maps, $I_{mk}{}^\star$ is the solution in the k-space. Integrating equations (6) and (7) yields

$$\xi FSI_m{}^\star = FSI_m{}^\star \dots\dots\dots\dots\dots\dots\dots\dots\dots\dots (8)$$

Sensitivity maps are estimated through eigenvalue decomposition of operator ξ, performing inverse Fourier

transform on equation 4.40

$$F^{-1}\xi FSI_m{}^{\star} = SI_m{}^{\star} \dots\dots\dots\dots\dots\dots\dots\dots\dots\dots (9)$$

Assuming $F^{-1}\xi F = v$, eigenvalue decomposition can be further simplified through smaller eigenvalue decomposition for v in the image domain. Thus equation (9) simply becomes

$$vSI_m{}^{\star} = SI_m{}^{\star} \dots\dots\dots\dots\dots\dots\dots\dots\dots\dots (10)$$

or, at position r where the image $I_m{}^{\star}$ has non-zero value

$$v_r S_r = S_r \dots\dots\dots\dots\dots\dots\dots\dots\dots\dots (11)$$

Sensitivities are computed through eigenvalue decomposition of v_r , by selecting the eigenvectors correspond to "eigenvalue= 1". Sometimes, errors in acquisition yield the possibility of multiple eigenvectors for "eigenvalue= 1", resulting in computing a set j=1, 2, 3,…, Z_r of sensitivity maps s_l^j based for multiple images I_m^j, equation (1) this is represented as

$$u_l = RF \sum_j s_l^j I_m^j \dots\dots\dots\dots\dots\dots\dots\dots\dots\dots (12)$$

Finally following optimization problem is proposed in ESPIRiT to obtain the final MR image

$$P\left(I_m^j\right) = \min_{I_m^j} \sum_l \left\| u_l - RF \sum_j s_l^j I_m^j \right\|_2^2 + \lambda \sum_j W\left(I_m^j\right) \dots\dots\dots\dots\dots\dots\dots (13)$$

L_1 regularization term in a wavelet basis for $W(I_m^j)$ is usually chosen, which makes the problem an L_1 ESPIRiT framework. The pointwise root of sum-of-squares on I_m^j is performed to obtain the final image. The proposed method aims to overcome the limitations of GRAPPA-based methods, i.e. SPIRiT by implementing sensitivity information to estimate MR image, also saves the pre-computation of coil maps through reference scanning. It paves a way to compute sensitivity maps from auto-calibration data, though some errors mentioned earlier resulting a set of sensitivity maps from a set of multiple images are estimated, ultimately pMRI reconstruction is done by performing the SOS operation which may result from inferior noise performance than other pure sensitivity-based methods.

B. Formulation of Convex ESPIRiT

From the proposed coil-by-coil reconstruction method proposed in equation (13), the final MR image is acquired by performing SOS recombination of all the reconstructed coil images

$$I_{mp} = \sqrt{\sum_{j=1}^{L} |I_m^j|^2} \dots\dots\dots\dots\dots\dots (14)$$

where L=total number of coils.

In this sub-section, the proposed method of ESPIRiT in equation (13) has been combined with a proposed convex optimization in [13] to replace the SOS recombination process stated in equation (14).

Bearing in mind that the final reconstructed image I_{mp} in (14) is magnitude only function, it is likely to implement a convex solution space for the magnitude image and the sensitivity encoded functions I_m^j, which can further be derived into a convex optimization formulation of the image reconstruction. An instinctive reflection of the convex solution space is discussed herewith.

Let $I_m^0 \in {\mathbb{R}_+}^{N\times N}$ be the magnitude representation of the final MR image I_m. As the magnitudes of the sensitivity maps are bounded due to bounded inductances of the coils, a constant entity cab be approximated as $B_l \in {\mathbb{R}_+}^{N\times N}$, such that $|Z| \preccurlyeq B$ for each coil $l = 1, 2, \dots, L$. It follows that

$$|I_{ml}| \preccurlyeq B_l \odot I_m^0, for\ l = 1, 2, \dots, L \dots\dots\dots (15)$$

If I_m^0 and I_m^j are measured as the solution entities, the inequalities in (15) interpolate into a convex hull comprising the solutions of I_m^0 and I_m^j , with carefully selected constant bound vectors B_l. This solution space delivers a basis for the convex optimization tactic for the final pMR image. It is, however, well-known that the global solution space only occurs for the magnitude image I_m^0 but not for any other real or complex-valued image vectors.

Selecting the appropriate boundary matrix can be complicated, but tapping an element-wise penalty which has positive magnitude with initial guesstimate on estimated weights Z can provide a suitable B.

$$min_{B,\delta} \|B - Z - \delta\|_2^2,\ subject\ to\ \ \delta \succcurlyeq 0 \dots\dots (16)$$

Now let's emphasize the bi-linear inequalities in (15). Resembling B for each coil in (16) re-forms problem (15) into no longer bi-linear. Considering the final MR image I_m^0 to be sparse in some transform domains and also non-negative, following convex optimization can be implemented over the results of ESPIRiT in equation (13).

$$\min_{I_m^0} \|WI_m^0\|_1\ \ subject\ to\colon I_m^0 \succcurlyeq 0, \left|I_m^j\right| \preccurlyeq B_l \odot I_m^0 \quad (17)$$

Where W signifies a universal wavelet transformation matrix and adopting that the wavelet transformed image vector WI_m^0 indicates a sparse domain.

The unconstraint Lagrangian form of the L_1 the regularized optimization problem (17) can be written as

$$\min_{I_m^0, q_l} \frac{1}{2}\left\|B_l \odot I_m^0 - |I_m^j| - q_l\right\|_2^2 + \frac{\alpha}{2}\|WI_m^0\|_1$$
$$subject\ to: I_m^0 \geqslant 0, q_l \geqslant 0 \ldots\ldots\ldots\ldots\ldots\ldots\ldots\ldots \quad (18)$$

Where, $q_l$is a non-negative element-wise penalty to shove $|I_m^j|$ always within the borderline of the convex solution region.

III. Experimental Setup

Two different sets of the dataset have been implemented to test the proposed method with traditional ESPIRiT reconstruction.

A. Data Acquisition

The initial dataset is a single slice in-vivo brain data set of a healthy human volunteer, the raw form of the dataset is available in [14]. This data was attained on a 3 Tesla SIEMENS Trio scanner with an 8-channel head array and an MPRAGE (3D Flash with IR prep.) sequence. The scanning parameters were TR/TE = 2530/3.45 ms, TI = 1100 ms, data resolution N×N = 256×256, flip angle = 7°, slice thickness = 1.33 mm and FOV = 256×256 mm^2. The data procurement was done in the Cartesian coordinate system and the fully acquired k-space data have been also manually subsampled by the pattern of uniform sampling with additional auto-calibration signal (USACS) lines along the phase encoding direction. The fully acquired k-space data are manually and uniformly subsampled at the nominal hastening rate, denoted by $\boldsymbol{f\_nom}$, together with supplementary 36 auto-calibration signals (ACS) lines in the central k-space region along the phase encoding direction to form the under-sampled k-space data pattern. Two sets of under-sampled data at $\boldsymbol{f\_nom}$ = 4 and 8 have been obtained. Considering the added 36 ACS lines, the corresponding net under sampling rates, denoted by $\boldsymbol{f\_net}$, of the data sets are $\boldsymbol{f\_net}$ = 2.56 and 3.76.

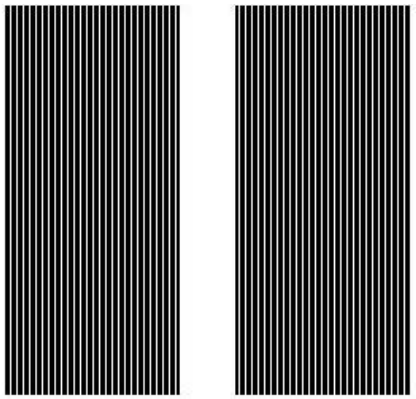

Fig. 1. USACS under-sampling pattern with $\boldsymbol{f\_net}$ =2.56 ($\boldsymbol{f\_nom}$ = 4)

The second one is of a phantom which was simulated 100 times and was scanned on a 3 Tesla SIEMENS machine with a 32-channel head using true fast imaging (TFI) with steady-state precession sequence (TrueFISP). The parameters of the scan were TR/TE = 11/6.5 ms, data resolution N×N = 256×256, flip angle = 60° and FOV = 162 × 162 mm^2. The assimilated k-space datasets are in the Cartesian system and consistently subsampled at the nominal rate of $\boldsymbol{f\_nom}$ = 4 and 8. The subsampled data along with the 32 additional ACS lines in the central k-space region along the phase encoding direction created a subsampled k-space dataset with net undersampling rate $\boldsymbol{f\_net}$ = 2.67 and 4.

B. Computational Setups

All the computational methods stated in the above discussions have been programmed on MATLAB (Math-Works, Natick, MA, USA). The implementation of the optimization problem given in equation (18) has been applied using the iterative algorithm proposed in [15]. The least-squares routine 'LSQR' in MATLAB [16] has been adopted to solve the non-negative sub-problem. The 2-D fast Fourier transform routine "fft2" was applied for faster and memory unloading of DFT operations. For wavelet domain in the L1 wavelet regularized reconstruction, Donoho's Wavelab codes [17] have been applied. Haar transform has been selected for the wavelet transform vector **W** for all the Cartesian datasets. Values of regularization parameters such as α are empirically chosen in the optimization algorithm for reconstruction of the *in vivo* as well as the phantom data sets.

For ESPIRiT, codes provided by respective authors in [18] have been used to generate pMRI reconstruction results for comparison.

To evaluate the reconstruction performance, the reconstructed images, denoted by I_m^0, are compared with the image reconstructed from fully acquired data samples, which is denoted as I_{SOS}. The normalized mean square error (NMSE) is defined as

$$e_{NMSE} = \frac{\left\|I_m^0 - I_{SOS}\right\|^2}{\|I_{SOS}\|^2}$$

IV. Results and Analysis

This segment represents the simulation results data. Firstly, the *in vivo* brain image from fully acquired samples is displayed as the reference image for comparison. Then the pMRI reconstructed images using the proposed convex formulation in (18) and the original ESPIRiT coil-array recombination method denoted by equation (14) for different nominal reduction factors has been publicized for comparison.

For each reduction factor, error images for both have been estimated and have been displayed along with the reconstructed images for the assessment objective.

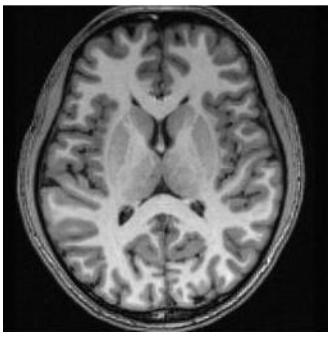

Fig. 2. In vivo brain image from the fully acquired dataset

Fig. 2 has been restored from the fully attained k-space data using inverse Fourier transform routine in MATLAB. Fig. 2 is set to be the reference image for comparing reconstruction abilities.

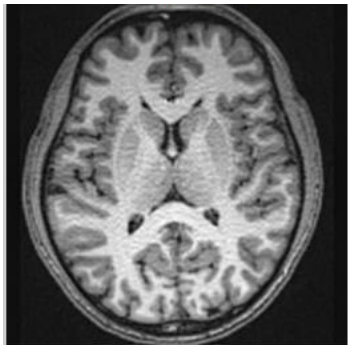

Fig. 3. Reconstructed in vivo brain image by ESPIRiT, for $\boldsymbol{f\_nom} = 4$

Fig. 3 embodies the restored pMR image for a nominal reduction factor of "4" (net reduction factor=2.56). The stated formula in Eq. (13) has been implemented and then followed by the SOS reconstruction given in (14) to achieve Fig. 3.

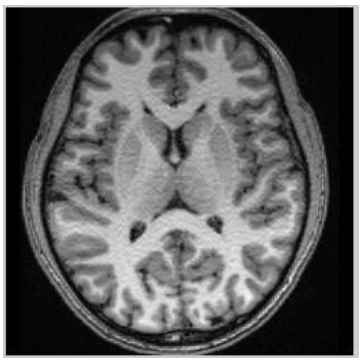

Fig. 4. Reconstructed in vivo brain image by proposed convex optimization formula following SPIRiT, for $\boldsymbol{f\_nom} = 4$

However, Fig. 4 has been reconstructed by substituting the SOS reconstruction with the convex optimization method proposed in (18). Though it is very apparent that both the images in Fig. 3 and Fig. 4 are very alike, upon closer examination a minor discrepancy in accumulated noise can be detected. In Fig. 3 the noise in the central area of the image is more prominent than Fig. 4.

It is obvious that from reconstructed images, the delicate difference is hard to find. To overcome that, error images have been obtained for both processes. Error image is projected by subtracting the reconstructed image (from subsampled data), from the SOS image (from the fully acquired dataset).

Fig. 5. Error image for ESPIRiT by SOS, for $\boldsymbol{f\_nom} = 4$.

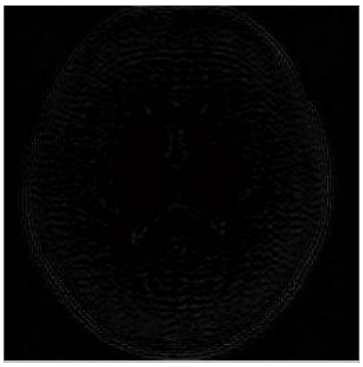

Fig. 6. Error image when SOS is replaced by convex optimization, for $\boldsymbol{f\_nom} = 4$.

After closely reviewing the error images in both Fig. 5 and Fig. 6 respectively, the superiority of the proposed convex method becomes more ostensible. Fig. 5 has brighter error pixels (indicating accumulating noise during reconstruction), whereas Fig. 6 has some marginal error pixels on the right side as well bottom left corner with very negligible grey values.

For quantitative comparison, normalized mean square error e_{NMSE} has been calculated using the aforementioned formula. Although the mean square error is not gold-standard in the MRI community for

evaluation of simulation-based reconstruction results. This method often yields different estimations from simulation to simulation in pMRI reconstruction. But for the ease of the readers, a means square error-based comparison chart has been added. In Table 1, each e_{NMSE} value has been accomplished after averaging three simulation runs and the highest error result has been also stated.

TABLE I
NMSE VALUES OF RECONSTRUCTED IMAGES BY ESPIRIT SOS AND BY PROPOSED FORMULA AT DIFFERENT REDUCTION FACTORS

f_nom	ESPIRiT SOS (Average)	ESPIRiT SOS (Highest)	Proposed Method (Average)	Proposed Method (Highest)
4	0.0055	0.0061	0.0044	0.0052
8	0.0096	0.0101	0.0084	0.0090
12	0.0114	0.0119	0.0099	0.0106

In the case of NMSE comparison, Table 1 also depicts that the proposed formula in (10) replacing the SOS in (6) can yield better results. But it is noted that NMSE results can't be taken for granted as results will vary if the images are reconstructed in a different device.

As conferred earlier SOS recombination often results in inferior Signal to Noise or SNR performance in the final MR image, a thorough investigation of SNR performances is carried out using the *in vivo* brain image and the phantom image. g-maps for both the images have been assessed to extricate the SNR performances of SOS and the proposed convex optimization method.

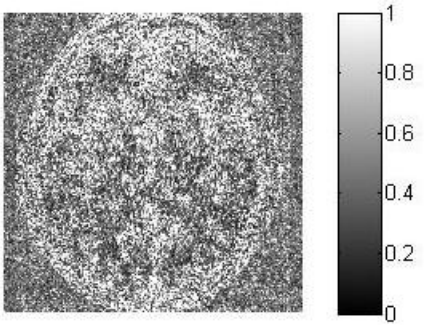

Fig. 7. g-factor maps remodeled for subsampled *in vivo* brain data using ESPIRiT SOS, $\boldsymbol{f\_nom} = 8$

For thorough SNR analysis using *in vivo* brain dataset, random noise with fixed variance has been added to the reference brain data. Then the data has been subsampled as described in section III-A and then reconstructed using ESPIRiT and the proposed convex optimization method. Following pMRI reconstructions, g-factor maps are estimated for both the methods as described in [19]. Fig. 7 shows the g-maps for the reconstructed subsampled *in vivo* brain dataset utilizing ESPIRiT for $\boldsymbol{f\_nom} = 8$. The brighter (closer to 1) grey values generally portray higher noise in the reconstruction process.

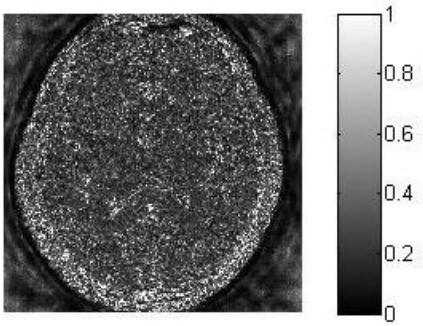

Fig. 8. g-factor maps remodeled for subsampled in vivo brain data using proposed convex optimization replacing SOS, $\boldsymbol{f\_nom} = 8$

Fig. 8 demonstrates the g-maps for reconstructed *in vivo* brain image using proposed convex optimization in Eq. (18) for the same subsampling measures $\boldsymbol{f\_nom} = 8$. This image comprises grey values with lesser magnitudes compared to Fig. 7, which interprets less noise accumulation related to SOS coil-by-coil reconstruction. Though these g-maps are estimated from single pMRI reconstruction, which does not guarantee the most precise g-maps comparisons. For more precise analysis, the phantom dataset has to be implemented. The detail of phantom scanning has been described in section III-A and the phantom image from the fully sampled dataset is displayed in Fig. 9.

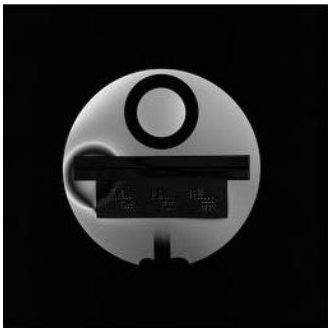

Fig. 9. Phantom image reconstructed from full data

For g-factor maps evaluation using phantom data, 100 sets of random noise matrices have been created using the "Randn" routine in MATLAB. Then the random noise matrices are coagulated with the 100 sets of phantom data to generate 100 sets of noise polluted phantom images. These phantom images are subsampled as stated in section III-A and reconstructed using ESPIRiT and the proposed convex optimization

method. g-factor maps are obtained for both methods and then averaged to harvest the final g-map image. The g-map images from phantom data are revealed in RGB format for the better consideration of their variances.

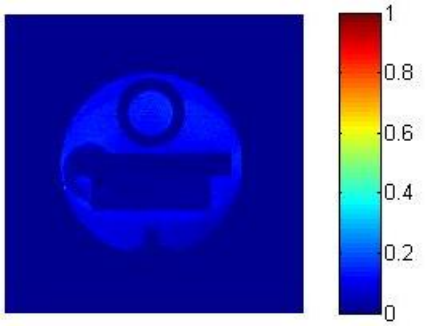

Fig. 10. g-maps obtained for phantom datasets using ESPIRiT multiple array coils recombinations, $\boldsymbol{f\_nom} = 4$

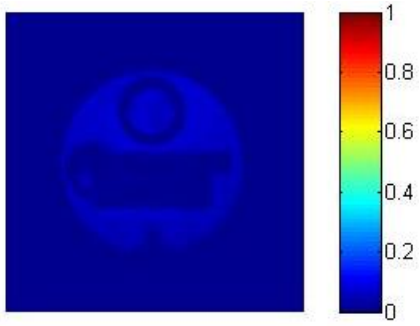

Fig. 11. g-maps obtained for phantom datasets using convex hull based proposed optimization method, $\boldsymbol{f\_nom} = 4$

In Fig. 10, a g-map image is obtained from the 100 sets of phantom images with additionally added noise matrices, reconstructed using ESPIRiT. If one opts for differences between Fig. 10 and Fig. 11, the g-map image in Fig. 10 is noticeably brighter than Fig. 11. As brighter pixels indicate a higher degree of accumulated noise, it can be safely presumed the SOS reconstruction used by ESPIRiT can yield a buildup of more reconstruction noise. Another fact should be realized is that less noise in the phantom image compared to *in vivo* brain image. This primarily can be interconnected to two factors. Firstly, *in vivo* images are more prone to collect noise throughout scanning and calibration than phantom images. Secondly, a single set of data has been taken to obtain g-factor maps for *in vivo* data which is not the typical norm. Moreover, *in vivo* comparison has been done to give some idea about noise performance differences between ESPIRiT and upgraded ESPIRiT by convex optimization.

V. Conclusion

The proposed convex-hull region approximated optimization approach to pMRI coil-by-coil recombination aims to improve the inherent shortcomings of coil-by-coil reconstruction algorithms which implements sum-of-square operation to get the final MR image. The proposed method needs to be implemented in a two-step procedure. In first, coil images are reconstructed using traditional and popular coil-by-coil reconstruction techniques i.e. GRAPPA, SPIRiT. These conventional algorithms depend indirectly on coil sensitivities and based on the postulation that coil maps are uniform. The exceptionality of ESPIRiT is it's also somehow linked to coil sensitivities through the extraction process of Eigenvalues. Though depending less on the presumption that coil sensitivities are uniform rather than linking coil maps with Eigen value-based optimization for the reconstruction process, gives ESPIRiT an upper hand over conventional coil-by-coil reconstruction methods which implement sensitivity data implicitly. But, the limitations of SOS recombination persist. The proposed method in this work is based on the presence of a convex hull in the coordinate system of the magnitude image and each of the sensitivity encoded coil images, which can be constructed using a priori information of upper bound vectors on the calibration data. Such a technique opts out any non-convex complicacy and permits a globally optimal solution for the pMRI reconstruction. It has been already observed through various comparisons in [19] that replacing SOS in SPIRiT by convex optimization can yield superior reconstruction performances. Though the proposed formula puts a toll on computational time but is manageable due to reconstruction time in computational machines do not have any effect on scanning length. As computational processing power is increasing with time, lengthy computational would not be an issue in the future.

Acknowledgment

The author would like to convey his gratitude to Dr. Kamlesh Pawer, Monash University Biomedical Imaging Lab (*https://www.monash.edu/researchinfrastructure/mbi/home*) for providing the raw noise-contaminated phantom data which has been used in the experimentation without any copyright complaint.

References

[1] "MRI Scans: All You Need To Know", Medical News Today, https://www.medicalnewstoday.com/articles/146309#what-is-an-mri-scan, 2018 [accessed: July 2018].

[2] P. B. Roemer, W. A. Edelstein, C. E. Hayes, S. P. Souza, and O. M. Mueller, "The NMR Phased Array," Magnetic Resonance in Medicine, vol. 16, pp. 192–225, 1990.

[3] M. Griswold, P. Jakob, R. Heidemann, M. Nittka, V. Jellus, J. Wang, B. Kiefer, and A. Haase, "Generalized Autocalibrating Partially Parallel Acquisitions (GRAPPA)," Magnetic Resonance in Medicine, vol. 47, pp. 1202–1210, 2002.

[4] Z. Chen, J. Zhang, R. Yang, P. Kellman, L. A. Johnston, and G. F. Egan, "IIR GRAPPA for Parallel MR Image Reconstruction," Magnetic Resonance in Medicine, vol. 63, pp. 502–509, 2010.
[5] M. Lustig and J. M. Pauly, "SPIRiT: Iterative Self-consistent Parallel Imaging Reconstruction from Arbitrary k-Space," Magnetic Resonance in Medicine, vol. 64, pp. 457–471, 2010.
[6] M. Murphy, M. Alley, J. Demmel, K. Keutzer, S. Vasanawala, and M. Lustig, "Fast -SPIRiT Compressed Sensing Parallel Imaging MRI: Scalable Parallel Implementation and Clinically Feasible Runtime," IEEE Transactions on Medical Imaging, vol. 31, pp. 1250–1262, 2008.
[7] D. S. Weller, J. R. Polimeni, L. Grady, L. L. Wald, E. Adalsteinsson, and V. K. Goyal, "Sparsity-Promoting Calibration for GRAPPA Accelerated Parallel MRI Reconstruction," IEEE Transactions on Medical Imaging, vol. 32, pp. 1325–1335, 2013.
[8] S. Park and J. Park, "Adaptive self-calibrating iterative GRAPPA reconstruction," Magnetic Resonance in Medicine, vol. 67, pp. 1721–1729, 2012.
[9] M. Uecker, P. Lai, M. J. Murphy, P. Virtue, M. Elad, J. M. Pauly, S. S. Vasanawala, and M. Lustig, "ESPIRiT-An Eigenvalue Approach to Autocalibrating Parallel MRI: Where SENSE Meets GRAPPA," Magnetic Resonance in Medicine, vol. 71, pp. 990–1001, 2014.
[10] M. Blaimer, F. Breuer, M. Mueller, R. Heidemann, M. A. Griswold, and P. Jacob, "SMASH, SENSE, PILS, GRAPPA: how to choose the optimal method," Top Magnetic Resonance Imaging, vol. 15, pp. 223–236, 2004.
[11] P. Beatty, "Reconstruction methods for fast magnetic resonance imaging," Ph.D. dissertation, Stanford University.
[12] M. A. Griswold, S. Kannengiesser, R. Heidemann, J.Wang, and P. Jacob, "Field-of-view limitations in parallel imaging," Magnetic Resonance in Medicine, vol. 52, pp. 1118–1126, 2004.
[13] C. Zhang and Ifat-Al-Baqee, "Parallel magnetic resonance imaging reconstruction by convex optimization", 2013 Third International Conference on Innovative Computing Technology (INTECH)in LONDON (IEEE Xplore), pp. 473-478, 2013.
[14] "Cartesian Dataset of Human Brain," http://maki.bme.ntu.edu.tw, 2005 (Accessed: April, 2012).
[15] T. Goldstein and S. Osher, "The split Bregman method for l1 regularized problems," SIAM Journal of Imaging Science, vol. 2, pp. 323–343, 2009.
[16] C. L. Lawson and R. J. Hanson, Solving Least Squares Problems. NJ: Prentice-Hall, 1974.
[17] J. Buckheit and D. L. Donoho, Wavelets and Statistics. Springer-Verlag, Berlin, 1996.
[18] M. Lustig, "ESPIRiT software", https://people.eecs.berkeley.edu/~mlustig/Software.html, (Accessed: September 2016).
[19] I. A. Baqee, "A Novel Approach of Obtaining Optimal Solution for Iterative Self-Consistent Parallel Imaging Reconstruction," *International Journal of Scientific technology and research*, vol. 9, issue. 9, pp. 100–107, 2020.

Ifat A. Baqee was born in Dhaka, Bangladesh. Dr. Baqee completed his Bachelor of Science (B.Sc.) in Electrical, Electronic, and Communication Engineering from Military Institute of Science and Technology (MIST), Mirpur, Dhaka under Bangladesh University of Professionals (BUP) in February 2009. After that, Dr. Baqee completed his Doctor of Philosophy (PhD) from the Swinburne University of Technology, Australia in 2016. The author's major field of study during the PhD tenure was computational image processing in the medical domain. After graduation, he first joined as a Lecturer at Stamford University Bangladesh in 2009. He served there up to 2012. After that, he moved to Australia to pursue his PhD degree. After completion of PhD, he came back to Bangladesh and joined as an Assistant Professor at the American International University Bangladesh (AIUB), Dhaka. He served up to 2019 in AIUB and then joined Southeast University, Tejgaon, Dhaka, Bangladesh. He is currently serving there as an Assistant Professor in the EEE Department. His previous and current research interests include but are not limited to computational image processing, neural processing, medical instrumentation, power system automation, control system, etc. He has a good number of international journal and conference paper publications under his name. Dr. Baqee is currently a member of the International Association of Computer Science and Information Technology (IACSIT). Dr. Baqee is also an active editorial member of the Australian Journal of Engineering and Innovative Technology (AJEIT).